Desalination and Water Treatment
www.deswater.com

doi:10.5004/dwt.2018.22603

116 (2018) 148–157
June

Comparative sorption study of cesium, cobalt and europium using induced gamma radiation polymeric nanocomposites

Mohamed Mahmoud E. Breky[a,*], Emad Hassan Borai[a], Magda Salah Eldin Sayed[a], Mohamed Mohamed Abo-Aly[b]

[a]*Hot Laboratories and waste Management Center, Atomic Energy Authority, Cairo 13759, Egypt, email: chemist_elbreky@yahoo.com (M.M.E. Breky), emadborai@yahoo.com (E.H. Borai), magdass7@hotmail.com (M.S.E. Sayed)*
[b]*Chemistry Department, Faculty of Science, Ain Shams University, Cairo, Egypt, email: aboalymo@yahoo.com (M.M. Abo-Aly)*

Received 6 October 2017; Accepted 6 June 2018

ABSTRACT

ZnO/poly (acrylamide-sodium styrene sulfonate) and Sb_2O_3/poly (acrylamide-sodium styrene sulfonate) nanocomposites were synthesized by in situ radiation-induced polymerization of sodium styrene sulfonate (SSS) onto poly acrylamide (PAAm) in the presence of ZnO and Sb_2O_3 nanoparticles. The prepared samples were characterized by X-ray diffraction (XRD), Fourier transform infrared spectroscopy (FTIR), the thermogravimetric analysis (TGA) and scanning electron microscopy (SEM). Batch studies were performed to estimate the influence of pH and contact time on the uptake of the nanoparticles and nanocomposites towards Cs^+, Co^{2+} and Eu^{3+}. The optimum pH for metal uptake were found to be at 8, 6 and 5for Cs^+, Co^{2+} and Eu^{3+} ions, respectively. The obtained results revealed that the removal percentage for the nanocomposite is higher than that of the corresponding nanoparticles and the removal efficiency of ZnO-nanocomposite is better than that obtained by Sb_2O_3-nanocomposite. The experimental maximum retention capacities for Cs^+, Co^{2+} and Eu^{3+} ions were found to be 100, 90 and 85 mg/g for ZnO-nanocomposite and 90, 75 and 72 mg/g for Sb_2O_3-nanocomposite, respectively. The results indicated that the ZnO-nanocomposite is the most promising resin and has higher potential use for efficient removal of Cs^+, Co^{2+} and Eu^{3+} ions from aqueous solutions over Sb_2O_3-nanocomposite.

Keywords: Polymer nanocomposites; Water treatment; Thermal properties; Sorption

1. Introduction

Due to water shortage, successful treatment of wastewater is a noteworthy essential for developing economies. This can be accomplished either by improvement of totally new strategies or by enhancing new material. Radioactive aqueous wastes that have hazardous long-lived radionuclides are usually treated using conventional methods such as chemical precipitation, ion exchange, evaporation, filtration and solvent extraction [1].

To prepare efficient materials for radioactive waste treatment, fillers have important roles in modifying the properties of various polymers and lowering the cost of their nanocomposites. The effect of fillers on the properties of nanocomposites depends on their level of loading, shape and particle size, aggregate size, surface characteristics and degree of dispersion. Recently, polymer-matrix nanocomposites have attracted much attention owing to their unique mechanical, optical, electric and magnetic properties, and strong interactions with the matrix resulting from the nanoscale microstructure and extremely large interfacial area between filler and matrix [2–4].

Zinc oxide (ZnO) is a promising candidate for the removal of contaminants and environmental remediation [5]. It has many surface active sites for the adsorption of heavy metal ions from an aqueous solution. Further, ZnO nanoparticles with a porous micro/nanostructure provide an ample surface area for the adsorption of heavy metal

*Corresponding author.

ions from contaminated water. Recently,there have been many reports on the adsorption of heavy metal ions using porous micro/nanostructured materials with different morphologies, such as nano-assemblies, nano-plates, hierarchical ZnO nano-rods and microspheres with nano-sheets as absorbents [6–8].

Lee et al. [9] prepared ZnO nanoparticles by solution-combustion method (SCM). The zinc oxide nanopowder showed higher removal rate of Cu^{2+} ions from the solution than titanium dioxide powders, P25 which, prepared by a homogeneous precipitation process at low temperature.

Oxides of antimony (OA) are a key member among all the other metal oxides from groups V to VI [10]. Literature reports that there are three phases of well-identified OA, which are diantimony trioxide (Sb_2O_3), diantimony tetraoxide (Sb_2O_4), and diantimony pentoxide (Sb_2O_5) [11]. The change in Gibbs free energy is the key parameter that affects the formation of the desired phase [12,13]. For instance, Sb_2O_5 does not exist above 525°C, only Sb_2O_3 and Sb_2O_4 are formed. Literature proves that nanoparticles of OA possess excellent properties as compared to bulk OA, for example, a higher refractive index [14,15], higher abrasive resistance, higher proton conductivity [16,17], excellent mechanical strength [18], and higher absorbability [19].

In general, OA nanoparticles can be synthesized via several methods, which can be classified according to the starting material for synthesizing nanoparticles. There are three main groups of starting material namely antimony trichloride ($SbCl_3$), antimony (Sb), and slag. For $SbCl_3$ as a starting material, microemulsion [20], solution phase reduction [21], hydrothermal [22,23], γ-ray radiation-oxidization [24] and biosynthesis [25] methods have been used. Poly thiophene–dodecyl benzene sulfonate (PTh–DBSNa)/Sb_2O_3 nanocomposite was chemically prepared in aqueous media and it was employed for the removal of lead ions from the aqueous solution [26]. Antimony phosphate nanoribbons were synthesized and characterized using different techniques. The synthesized nanophosphate was studied for its efficiency as sorbent for uptake of various metal ions including uranyl ion. The results indicated that a clean separation of uranyl ion from its various binary mixtures could be achieved at an optimized pH of 4.5 and equilibration period of 1 h using 0.1 g of the sorbent [27].

In recent years, polymer nanocomposites (PNCs) have attracted the attention of scientists and technologists in water purification due to improved processability, surface area, stability, tunable properties, and cost effectiveness. PNCs showed fast decontamination ability with high selectivity to remove various pollutants [28]. The advanced nanocomposite membranes could be designed to meet specific water treatment applications by tuning their structure and physicochemical properties (e.g. hydrophilicity, porosity, charge density, and thermal and mechanical stability) and introducing unique functionalities (e.g. antibacterial, photocatalytic or adsorptive capabilities) [29].

^{60}Co and $^{152+154}Eu$ radionuclide were successfully removed using the polymer composite ion exchanger, hydrous titanium oxide (TiO-OH) incorporated in polyacrylonitrile (PAN) from the aqueous solution [30]. Furthermore, the synthesis of TiO_2/P (AAm–SSS) nanocomposite was investigated and applied to remove Cs^+, Co^{2+} and Eu^{3+} metal ions from aqueous solution. The maximum experimental retention capacities for Cs^+, Co^{2+} and Eu^{3+} were found to be 120, 100.9 and 85.7 mg/g, respectively [30].

The present paper is oriented to synthesize functionalized polymeric nanocomposites that gather the advantages of both morphological structure of nanomaterial (such as high surface area) and the presence of function groups loaded on the polymer (sulfonate groups). Simple and effective method was used to synthesize ZnO/P (AAm-SSS) and Sb_2O_3/P (AAm-SSS) nanocomposites. These materials should provide several advantages over the individual organic and inorganic materials. Moreover, the effect of the sorption parameters were systematically investigated in order to improve the sorption efficiency of Cs^+, Co^{2+} and Eu^{3+} ions from aqueous solutions.

2. Experimental

2.1. Chemical and Reagent

Zinc acetate dihydrate ($Zn(C_2H_3O_2)_2{\cdot}2H_2O$) was purchased from Merck Co., Antimony tricholride was purchased from Sigma Aldrich Co. Polyacrylamide (PAM), and sodium hydroxide were purchased from alpha Co., Ltd., China. N,N′-methylenebisacrylamide (MBA) was purchased from Merck Co., Sodium styrene sulfonate (SSS) was purchased from Sigma Aldrich Co. Acetone and Ethanol were purchased from Alnaser Co., Egypt.

2.2. Synthesis of ZnO nanoparticles

In a typical procedure, 6.58 g $Zn(C_2H_3O_2)_2{\cdot}2H_2O$ was first dissolved in 150 ml of distilled water with continuous stirring until a homogeneous solution was obtained. 0.2 M of NaOH was added drop by drop until the pH of the solution reached 12. The white precipitate was obtained with continuous stirring at 70°C for 1 h and was then cooled to room temperature. The precipitate was filtered, rinsed with distilled water and ethanol several times, then collected and calcined at 300°C for 2 h.

2.3. Synthesis of Sb_2O_3 nanoparticles

Sb_2O_3 nanoparticles were prepared by adding 10.03 g of antimony trichloride ($SbCl_3$) to dilute HCl solution (pH = 1.35) to avoid the hydrolysis of $SbCl_3$. Ammonium hydroxide, 30%, was added to the $SbCl_3$ solution till white precipitate was formed. The mixture was magnetically stirred for 30 min at the pH range of 8.5–9.0, followed by filtering, washing several times with distilled water and anhydrous alcohol and drying at 200°C for 2 h.

2.4. Synthesis of ZnO/P (AAm-SSS) and Sb_2O_3/P (AAm-SSS) nanocomposites

ZnO/P(AAm-SSS) and Sb_2O_3/P(AAm-SSS) nanocomposites were prepared according to the following procedures: 0.75 g of SSS was dissolved in 5 ml distilled water while 0.02 g of MBA was dissolved in 5 ml distilled water and poured to the SSS solution, then stirred for 10 min. After that, different amounts of ZnO and Sb_2O_3 nanoparti-

cle powders were dispersed individually in the above mentioned solution. The mixture was stirred vigorously for 30 min. Known amount of poly acrylamide (0.03 mg/10 ml) was then added under nitrogen atmosphere. After stirring for 20 min at 25°C, the mixture was subjected to Gamma cell ^{60}Co γ-irradiator at dose 20 kGy. The resulting rubbery gel was removed from the reaction vessel; cut up into small pieces and washes several times by acetone and dried at 60°C until constant weight.

2.5. Characterization

X-ray diffraction spectra of the powders were recorded at room temperature using a powder diffractometer Bruker AXS D8 Advance, Germany with Cu Kα radiation source (λ = 1.5406 Å) and 2θ in the range 10–80°. The average crystallite size was determined according to the Scherrer equation [31].

$$D = 0.9\,\lambda/(\beta \cos\theta)\ldots \quad (1)$$

where λ is the X-ray wavelength, θ is the Bragg angle of the peak of interest and β is the line broadening measured from the peak width at half height.

All IR spectra were recorded using a Jasco FT/IR-460 pluse, Japan. Samples were measured on KBr disc (1:10, sample/KBr), using 16 scans per sample at resolution of 4 cm^{-1} over the range 4000–400 cm^{-1}.

Thermogravimetric analysis (TGA) was carried out by using TA 50 Shimadzu, Japan. The temperatures were cycled at a constant rate of 20°C/min from ambient temperature to 800°C.

Magnification SEM micrographs of nanocomposites particles were characterized by field emission scanning electron microscope (FESEM, Quanta FEG 250, Holland,) to analyze the fine structures in a single particle and characterize the morphology.

2.6. Adsorption procedure

Co^{+2} and Eu^{+3} stock solutions were prepared from $CoCl_2{\cdot}6H_2O$ and $EuCl_3{\cdot}6H_2O$ by dissolution of desired weight in 0.1% nitric acid. Non-radioactive CsCl was used as a carrier for radioactive Cs^+. Kinetic and adsorption capacity experiments were conducted in a series of 15 ml polyethylene tubes containing 0.05 g of the nano-structured materials ZnO, ZnO/P(AAm-SSS), Sb_2O_3 and Sb_2O_3/P(AAm-SSS) with 10 ml of 100 mg L^{-1} metal ions solution. The desired pH value of the aqueous solution was adjusted by acetate buffer prepared at the desired pH. The nanostructured materials/aqueous solution mixture was shaken at 25°C. Solid/liquid phases were then separated by centrifugation (4,000 rpm) then filtered through a 0.45 μm filter membrane (super pure filter, Sartorius Company).

2.7. Metal analysis method

The unknown concentrations of metal ions (Co^{2+} and Eu^{3+}) were measured by forming colored complexes using 4-(Pyridyl-2-azo) resorcinol (PAR) as sensitive coloring reagent. 1 ml of the metal solution was placed into the 10 ml standard flask and then 1 ml of PAR and 1 ml of buffer solution (pH: 8.0 and 6.0 for Co (II) and Eu (III), respectively) were added and diluted to 10 ml with water. The absorbance was measured at 510 nm and 515 for both Co^{2+} and Eu^{3+}, respectively. The absorbance value was then compared with the calibration curve of the standard metal ions at different concentrations.

Radioactive Cs^+ ions were measured by NaI scintillation detector connected to the multi-channel analyzer (Genne 2000, USA). The uptake percent (uptake %) of Cs was calculated from the following equation:

$$\text{Uptake \%} = (A_\circ - A)/A_\circ) \times 100\ldots \quad (2)$$

where $A_\circ$ and A are the activities expressed in counts per minute of 10 ml solution of the radioactive Cs before and after contacting with nanocomposite. The uptake percentage of both Co(II) and Eu(III) metal ions was calculated by the following equation:

$$\text{Uptake \%} = (C_\circ - C_{eq})/C_\circ \times 100\ldots \quad (3)$$

The capacity of metal adsorbed on nanoparticles and nanocomposite, q (mg/g), was calculated according the equation:

$$q = (C_\circ - C_{eq}) \times V/m\ldots \quad (4)$$

where $C_\circ$, C_{eq}, are the initial and finial metal ion concentrations in solution after equilibrium (mg/L). V and m are the volume of the solution (L) and the mass of nanoparticle and nanocomposite (g).

3. Results and discussion

3.1. Characterization of ZnO, Sb_2O_3 nanoparticles and polymeric nanocomposite

3.1.1. XRD analysis

Fig. 1 shows the XRD patterns of ZnO nanoparticles and ZnO/P(AAm-SSS) nanocomposite. Pattern (A) of ZnO nanoparticles showed a single phase of ZnO structure and the dominant peaks of nano-ZnO appear at 2θ angles of 31.7°, 34.3°, 36.12° and 56.5°.

Fig. 1B for ZnO/P(AAm-SSS) nanocomposite showed four dominant peaks corresponding to crystalline characteristic peaks at 2θ angles of 31.7°, 34.3°, 36.1° and 56.4°, which are analogous to the main characteristic peaks of nano-ZnO. The XRD results show that nano-ZnO was incorporated in the ZnO/P(AAm-SSS) nanocomposite. All the characteristic peak locations in the ZnO/P(AAm-SSS) nanocomposite were slightly shifted to lower angles compared with those of nano-ZnO. Also, Li et al. [32] have also, observed the shift of the peaks of TiO_2 in TiO_2/ Polyethersulfone (PES) hybrid membranes. This shift was most probably due to the interactions between TiO_2 and polyethersulfone (PES). Similarly, for ZnO/ P(AAm-SSS) nanocomposite, it was observed a slight shift in the peaks location due to the interactions between ZnO and P(AAm-SSS). The average crystallite size of ZnO in the nanocomposite was calculated by Scherrer equation and found to be 22.3 nm.

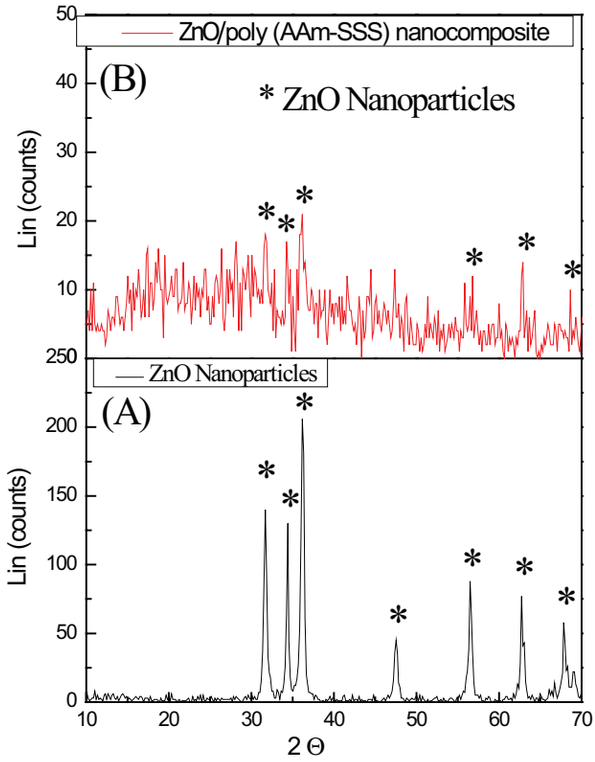

Fig. 1. XRD patterns of (A) ZnO nanoparticles calcined at 300°C and (B) ZnO/poly (AAm-SSS) nanocomposite.

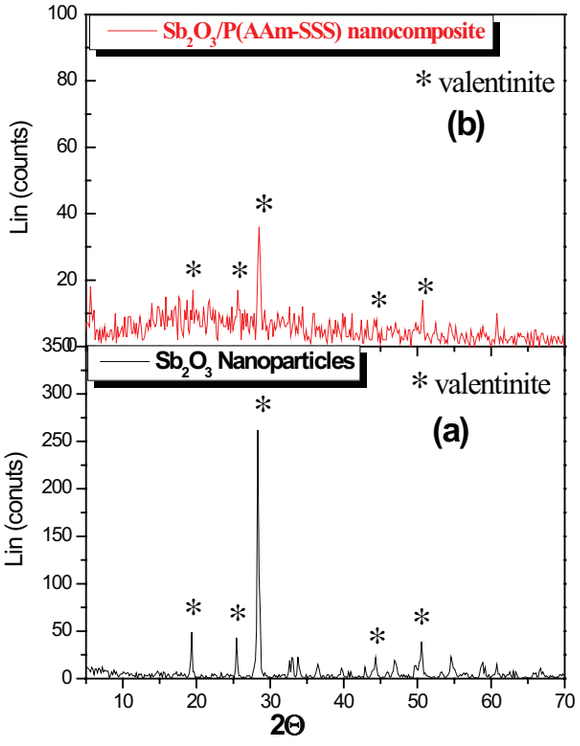

Fig. 2. XRD patterns of (a) Sb_2O_3 nanoparticles calcined at 200°C (b) Sb_2O_3/poly (AAm-SSS) nanocomposite.

The XRD of Sb_2O_3 nanoparticles and Sb_2O_3/P (AAm-SSS) nanocomposite are shown in Fig. 2. The XRD pattern of the Sb_2O_3 nanoparticles showed only the peaks of valentinite (orthorhombic polymorph) form, with no evidence for the presence of senarmontite form. The diffraction peaks centered at 2θ = 19.48°, 25.59°, 28.44°, 44.34° and 50.56° in pattern 2 (a) are similar to the peaks found in pattern 2 (b), which confirmed the existence of Sb_2O_3 (valentinite) nanoparticles in the P (AAm-SSS) matrix.

The average crystallite size of antimony trioxide in the nanocomposite was calculated by Scherrer equation, and found to be about 42.64 nm.

3.1.2. FTIR analysis

Structural investigations using FT-IR spectra, particularly in the fingerprint region (400–4500 cm^{-1}) are presented in Figs. 3 and 4.

For Fig. 3 (a) and (b), absorption peaks at 436.798 cm^{-1} and 423.298 cm^{-1} are attributed to the stretching vibrations of ZnO nanoparticle. The absorption peaks at 3437 cm^{-1} and 3433.64 cm^{-1} correspond to the stretching vibration of intermolecular hydrogen bond (O–H).

ZnO/P(AAm-SSS) and Sb_2O_3/P(AAm-SSS) spectra present the following absorption bands: 2922.59 and 2923 cm^{-1} corresponds to (st(C–C)), 1126.22 and 1125 cm^{-1} corresponds to (C–H, 1,4 substitution), and 1179.26 and 1186 cm^{-1} corresponds to st(S=O), associated to 4-styrene sulfonate group, and absorption bands at 1632.45 and 1530 cm^{-1}

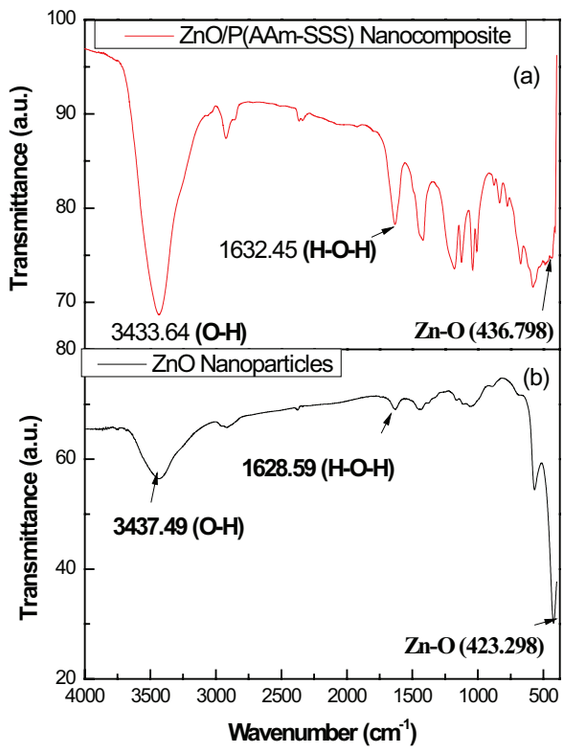

Fig. 3. FT-IR spectra of the prepared ZnO powder and ZnO/P(AAm-SSS).

corresponds to δ(NH_2), 1040.41 and 1040 cm^{-1} corresponds to st(C–N) related to acrylamide group and an overlapped band appear at 1632.45 and 1644 cm^{-1} associated to 1,4 substitution of aromatic ring and carbonyl stretching of amide for ZnO/P(AAm-SSS) and Sb_2O_3/P (AAm-SSS) nanocomposites, respectively [33].

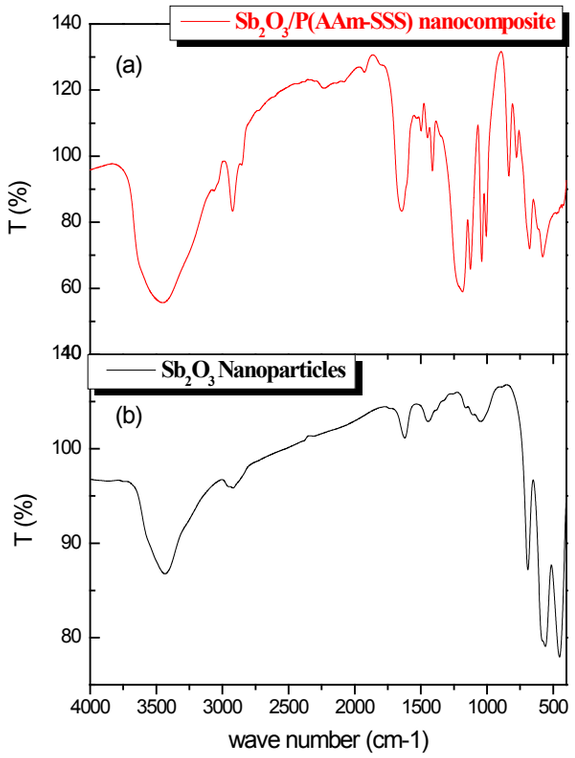

Fig. 4. FT-IR spectra of the prepared Sb_2O_3 powder and Sb_2O_3 /P (AAm-SSS).

Fig. 4a shows that the peaks at 473, 579 and 677 cm^{-1} are corresponding to symmetric and anti-symmetric Sb-O-Sb vibrations [34].

As shown in Fig. 4b, Sb_2O_3 nanoparticles exhibit characteristic bands located at 690, 559 and 452 cm^{-1} which corresponding to symmetric stretching, symmetric bending and asymmetric bending Sb-O-Sb vibrations of the valentinite form of SbO_3 trigonal pyramids with C_s or C_2 symmetry, respectively [35].

3.1.3. Thermal characterization

3.1.3.1. ZnO Nanoparticles

Fig. 5 shows the thermal behavior (TGA) of the as prepared ZnO nanoparticles. It can be seen that there are two pronounced mass loss steps in the temperature ranges 15–58°C and 175–323°C, respectively. The first weight loss is mainly attributed to the evaporation of surface adsorbed water, whereas the second one might be ascribed to the volatilization and combustion of organic species (acetate part) in sample. The first mass loss was 1.3%, while the second weight loss was 9%.

3.1.3.2. ZnO/P(AAm-SSS) nanocomposite

The thermal analysis results of the prepared ZnO/P(AAm-SSS) are illustrated in Fig. 6. The figure indicates that the P(AAm-SSS) and ZnO/P (AAm-SSS) nanocompsite show analogous thermal decomposition tendencies. The figure showed three weight loss steps. The P(AAm-SSS) polymer exhibited first decomposition between 25–160°C (15 % weight loss). For ZnO/P(AAm-SSS) nanocompsite, the first decomposition step between 25–175°C is accompanied by 17% weight loss. It can be attributed to water evaporation and organic impurities. The second decomposition is accompanied by 8% weight loss at (446–483°C) and (465–510) for ZnO/P (AAm-SSS) nanocomposite and P(AAm-SSS),

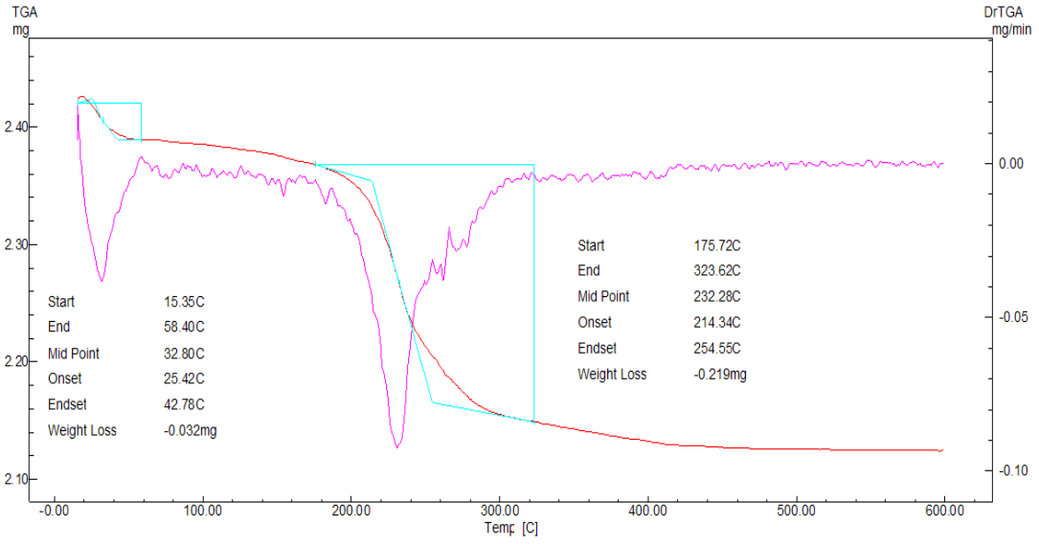

Fig. 5. TGA curve of ZnO nanoparticles.

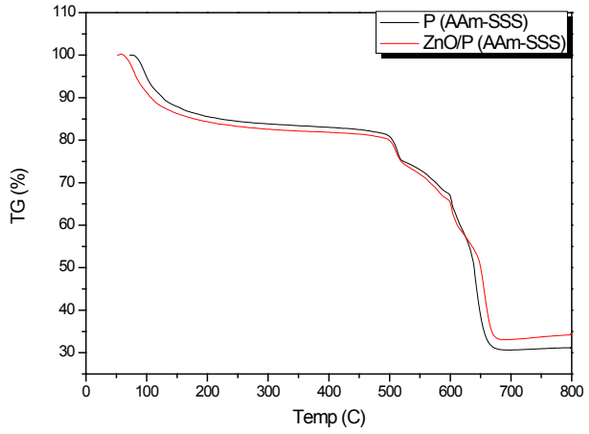

Fig. 6. TGA curves ofZnO/P(AAm-SSS) and P(AAm-SSS) nanocomposite.

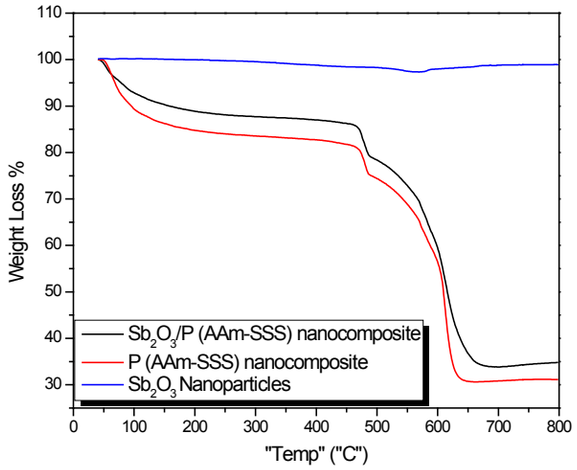

Fig. 7. TGA curves of Sb_2O_3 nanoparticles Sb_2O_3/P(AAm-SSS) and P(AAm-SSS) nanocomposite.

respectively. It can be attributed to the acrylamide moiety. The third decomposition is accompanied by 40% weight loss (578–685°C) and 40% (576–662°C) for ZnO/P (AAm-SSS) nanocomposite and P(AAm-SSS), respectively. These are attributed to the decomposition of styrene sulfonate groups.

From Fig. 6, the addition of ZnO nanoparticles to the polymer matrix enhance the thermal properties and shifted the thermal curve to higher values. These results were also in an agreement with Li et al. [32] and Wei et al. [36] whose observed that the addition of inorganic particles improved the thermal stability of polymer.

3.1.3.3. Sb_2O_3 Nanoparticles

The TG curve of Sb_2O_3 in air is shown in Fig. 7. Sb_2O_3 nanoparticles are stable in air up to 550°C above which temperature it starts absorbing oxygen to form Sb_2O_4. Between 550 and 700°C a net weight gain of 1% is observed and there is no further change in the mass of sample up to 800°C [37].

3.1.3.4. Sb_2O_3/P (AAm-SSS) nanocomposite

In Fig. 7, TGA profile of Sb_2O_3/P(AAm-SSS) nanocomposite and P(AAm-SSS) show three weight loss steps. The first step shows that the decomposition between 0–215°C, is accompanied by 12 and 14% weight losses for Sb_2O_3/P(AAm-SSS) nanocomposite and P(AAm-SSS), respectively. This is can be attributed to evaporation of water and organic impurities. The second decomposition (455–500°C), is accompanied by 6.5 and 8%weight losses for Sb_2O_3/P(AAm-SSS) nanocomposite and P(AAm-SSS), respectively, which attributed to the acrylamide moiety. The third decomposition (501–710°C), was accompanied by 44.5 and 43.5% for Sb_2O_3/P(AAm-SSS) nanocomposite and P(AAm-SSS), respectively. These losses are attributed to the decomposition of styrene sulfonate groups. On the other hand, 1% gain weight is attributed to conversion of Sb_2O_3 to Sb_2O_4. With the last decomposition step, the Sb_2O_3/P(AAm-SSS) nanocomposite is decomposed into sulfur dioxide and ammonium and Sb_2O_4. The total weight loss is 63 and 65.5% for Sb_2O_3/P(AAm-SSS) nanocomposite and P(AAm-SSS), respectively.

Based on the obtained results, it could be stated that the shifting in the thermal curve of Sb_2O_3/P(AAm-SSS) nanocomposite, is attributed to the addition of Sb_2O_3 nanoparticles which enhances the thermal stability of the polymer.

3.1.4. Morphology of ZnO/P(AAm-SSS) and Sb_2O_3/P(AAm-SSS) nanocomposites

The morphology of ZnO nanoparticles, ZnO/P(AAm-SSS), Sb_2O_3 nanoparticles and Sb_2O_3/P(AAm-SSS) nanocomposites are shown in Fig. 8. The size and homogeneity of particles are dependent on zinc oxide and antimony oxide. It can be stated that, the ZnO nanoparticles and Sb_2O_3 nanoparticles are not only dispersed on the surface of the polymer, but also embedded into the polymer matrix.

3.2. Effect of ZnO and Sb_2O_3 nanoparticles content on nanocomposite uptake

The effect of ZnO and Sb_2O_3 nanoparticles content incorporated into the nanocompsite on the adsorption behavior of the investigated metal ions has been tested. From Fig. 9, it can be seen that with the increase of nanoparticle concentration, the uptake percentage of Co^{2+} and Eu^{3+} increases firstly then decreases. This may attributed to the presence of hydroxyl groups on the nanoparticle surface that can synergistically interacted with the sulfonic acid groups on P(AAm-SSS) polymer chains. In this case, nanoparticles can be considered as a cross-linker in the reaction.

With the decrease of nanoparticles concentration lower than 0.06 g/10 mL, the solubility of nanocomposite increases, resulting in decrease the removal efficiency of Co^{2+} and Eu^{3+}. With the increase of nanoparticles concentration higher than 0.06 g/10 mL, the cross-linking density of the nanocomposite is significantly increased. Therefore, remaining structure network spaces left for Co^{2+} and Eu^{3+} sorption are decreased. The optimum concentration of nanoparticles was achieved at 0.06g/10 ml at which satisfactory uptake percentages were obtained (Fig. 9).

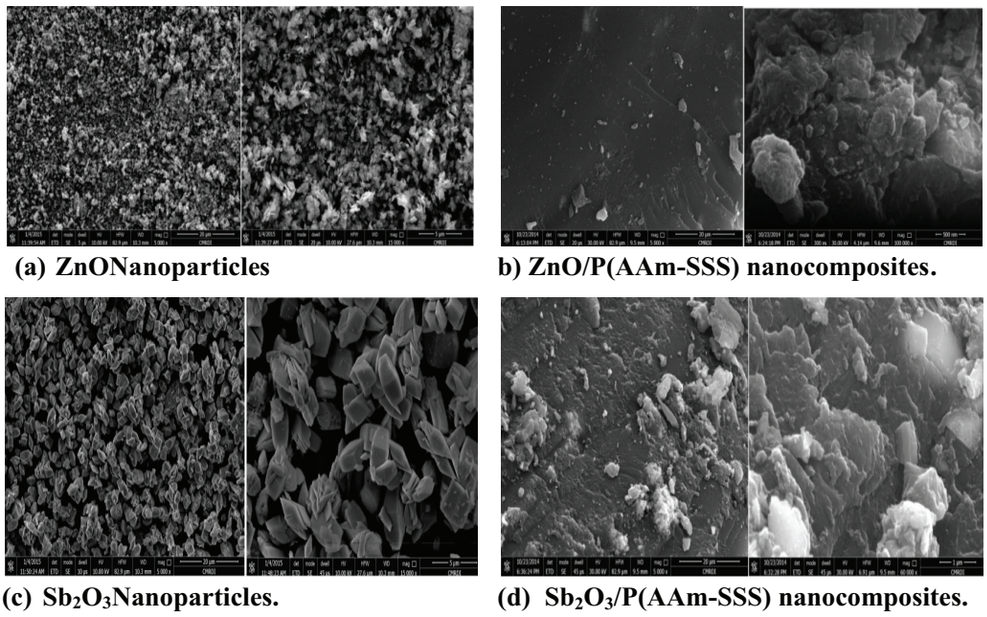

Fig. 8. SEM images of (a) ZnO nanoparticles, (b) ZnO/P(AAm-SSS), (c) Sb_2O_3 nanoparticles and (d) Sb_2O_3/P(AAm-SSS) nanocomposites.

3.3. Batch sorption experiments

Cs^+, Co^{2+} and Eu^{3+} were selected to represent mono, di and trivalent metal ions that mostly exist in radioactive waste solution. All experiments were carried out using radioactive Cs-137 and Co^{2+} and Eu^{3+}metal ions.

3.3.1. Effect of shaking time

The effect of shaking time on radioactive Cs^+, Co^{2+} and Eu^{3+} ions distribution have been tested to clarify its insights into reaction kinetics. The sorption kinetics of radioactive Cs^+, Co^{2+} and Eu^{3+} was studied at different time intervals ranging from 10 min to 24 h at constant V/M ratio.

As shown in Table 1, the equilibrium time for radioactive Cs^+ is reached at two hrs on the ZnO/P (AAm-SSS) and Sb_2O_3/P(AAm-SSS) nanocomposites. Table 1 shows the uptake efficiency of Co^{2+} and Eu^{3+} ions by ZnO, $Sb_2O_{3,\,ZnO}$/P(AAm-SSS) and Sb_2O_3/P(AAm-SSS) nanocomposites. The maximum uptake value for Co^{2+} and Eu^{3+} reached after three and two hrs for metal oxide nanoparticles and metal oxide/P(AAm-SSS) nanocomposites, respectively. The data indicated that the uptake percentage of Sb_2O_3 nanoparticles and Sb_2O_3/P(AAm-SSS) nanocomposite were lower than the corresponding values of ZnO, ZnO/P(AAm-SSS) nanocomposite. The presence of ZnO nanoparticles in P(AAm-SSS) nanocomposite enhanced the uptake process for radioactive Cs^+, Co^{2+} and Eu^{3+} ions, respectively.

3.3.2. Effect of pH

The pH of the aqueous solution has been identified as the most important variable governing metal adsorption.

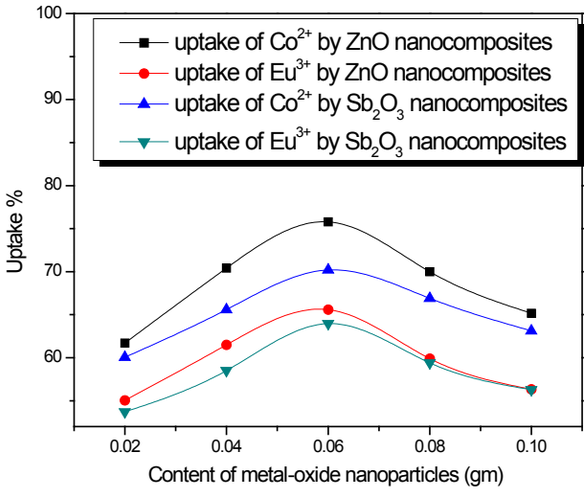

Fig. 9. Effect of ZnO and Sb_2O_3 nanoparticles content on uptake of Co^{2+} and Eu^{3+} (pH 4, Initial concentration 100 mg/L).

This is partly due to the fact that hydrogen ions themselves are strong competing ions and partly because the solution pH influences the chemical speciation of the metal ions as well as the ionization of the functional groups onto the adsorbent surfaces. The solution pH affects the surface charge of the adsorbents; hence it affects the adsorption process. Also, the active sites are closely associated with hydronium ions H_3O^+ may interact with the existing functional groups [38]. In order to evaluate the influence of pH on the adsorption capacity, the experiments were carried out at different pH ranging from 2–10, 2–8 and 2–6 for Cs^+, Co^{2+} and Eu^{3+} ions, respectively, with an initial Cs^+,

Table 1
Effect of contact time on adsorption of Cs^+, Co^{2+} and Eu^{3+} on ZnO, ZnO/P (AAm-SSS), $Sb_2O_{3\ and\ Sb2}O_3$/P (AAm-SSS) nanocomposite, $C_{(initial)}$ = 100 ppm, pH 4.0, m/v = 5 g L^{-1}

Time (min.)	ZnO			ZnO/P (AAm-SSS)		
	Cs^+ (ppm)	Co^{2+} (ppm)	Eu^{3+} (ppm)	Cs^+ (ppm)	Co^{2+} (ppm)	Eu^{3+} (ppm)
10	–	32.8	26.6	15.7	42.4	30.6
30	–	39.5	31.1	28.4	49.3	47.1
60	–	49.9	36.1	44.7	64.9	61.1
120	–	51.4	37.9	51.6	75.8	66.4
180	–	52.6	40.4	53.9	76.8	68.1
1440	–	53.2	40.6	54.1	78.1	68.1
	Sb_2O_3			Sb_2O_3/P (AAm-SSS)		
	Cs^+ (ppm)	Co^{2+} (ppm)	Eu^{3+} (ppm)	Cs^+ (ppm)	Co^{2+} (ppm)	Eu^{3+} (ppm)
10	–	30.7	16.9	12.5	40.5	28.6
30	–	34.6	20.8	25.6	53.1	39.6
60	–	41.3	29.09	38.7	64	55.4
120	–	41.7	30.7	43.7	69.8	63.97
180	–	42.1	32.2	45.5	70.2	64.2
1440	–	42.2	32.4	45.7	70.2	64.4

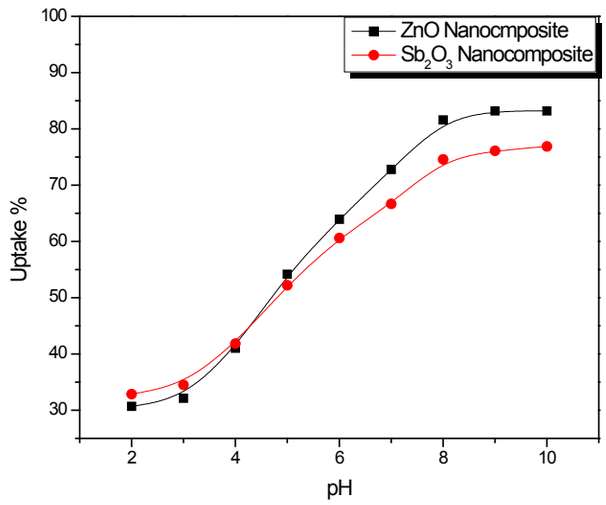

Fig. 10. Effect of pH on adsorption of radioactive Cs^+ on to ZnO/P (AAm-SSS) and Sb_2O_3/P (AAm-SSS) nanocomposite, adsorbent dosage: 5 g L^{-1}.

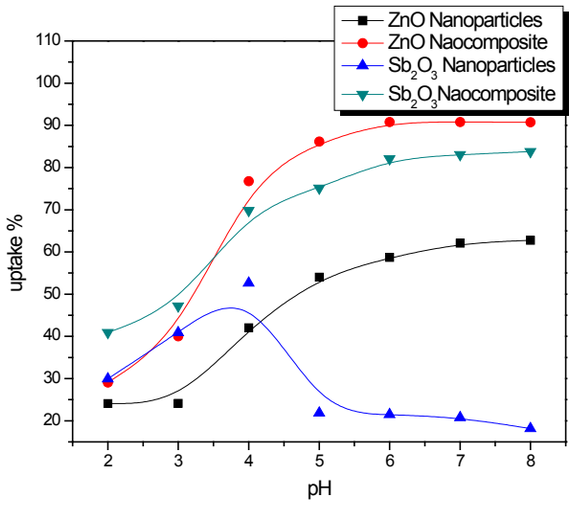

Fig. 11. Effect of pH on adsorption of Co^{2+} on ZnO, ZnO/P (AAm-SSS), Sb_2O_3 and $S_{b2}O_3$/P (AAm-SSS) nanocomposite, $C_{(initial)}$ = 100 ppm, m/v = 5 g L^{-1}.

Co^{2+} and Eu^{3+} ions concentration of 100 mg/L and a contact time of 120 min. These pH ranges are selected for each metal ion to avoid the metal hydrolysis. The results are shown in Fig. 10, 11 and 12 for Cs^+, Co^{2+} and Eu^{3+} ions, respectively.

As can be seen, all the uptake percentages of Cs^+, Co^{2+} and Eu^{3+} ions by ZnO/P(AAm-SSS) and Sb_2O_3/P (AAm-SSS) nanocomposite increase with increasing the solution pH and an optimum value was obtained at pH 8, 6 and 5 for Cs^+, Co^{2+} and Eu^{3+} ions, respectively. On the contrary, in the case of Sb_2O_3 nanoparticles, the uptake percentage of Co^{2+} increases with decreasing the solution pH and an optimum value was obtained at pH 4. The possible reason for pH 4 is the synergistic effect of surface complexation and ion exchange. Also, the more absorptive sites in Sb_2O_3 may also play an important role in the improvement of adsorption capacity.

3.3.3. Maximum retention capacity of Cs^+, $Co^{+2}$and Eu^{+3}

As shown in Fig. 13, the retention capacities of Cs^+, Co^{2+} and Eu^{3+} ions by ZnO/P(AAm-SSS) and Sb_2O_3/P(AAm-SSS) nanocomposites as a function of their concentration ranged from 100 to 1000 mg L^{-1} at the

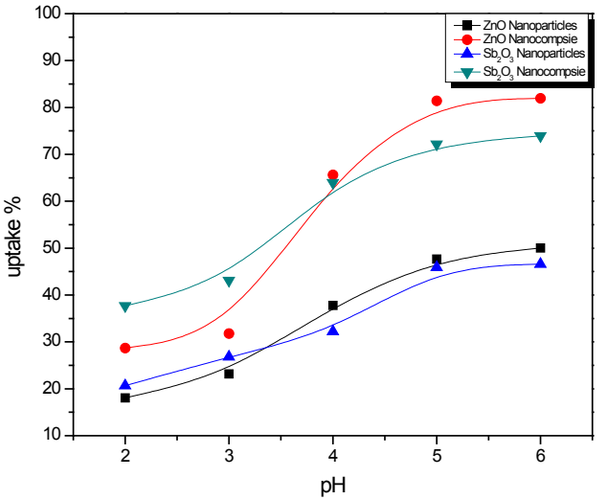

Fig. 12. Effect of pH on adsorption of Eu^{3+} on ZnO, ZnO/P (AAm-SSS), $Sb_2O_{3\ and\ Sb2}O_3$/P (AAm-SSS) nanocomposite, $C_{(initial)}$ = 100 ppm, pH 4.0, m/v = 5 g L^{-1}.

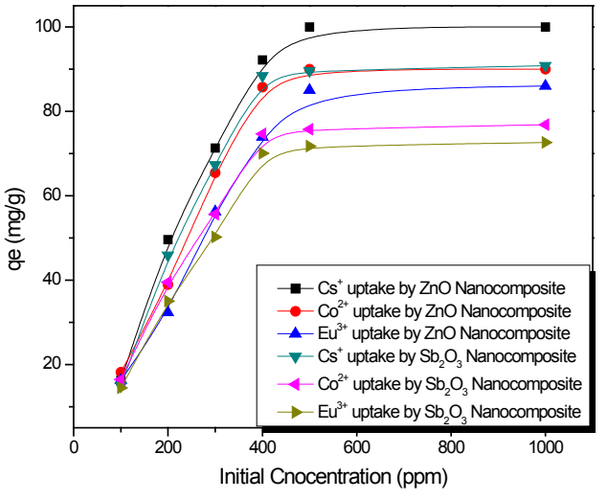

Fig. 13. Sorption isotherm of Cs^+, Co^{2+} and Eu^{3+} ions on ZnO/P(AAm-SSS) and Sb_2O_3/P (AAm-SSS) nanocomposites at pH 8, 6 and 5, respectively, m/v = 5 g L^{-1}.

corresponding optimum pH for each cation (at pH 8, 6 and 5 for Cs^+, Co^{2+} and Eu^{3+}, respectively) were investigated. The equilibrium capacity of Cs^+, $Co^{2+}$and Eu^{3+} ions increased with increasing amounts of metals ions added. The maximum metal adsorption capacity occurred by ZnO/P(AAm-SSS) was found to be 100, 90 and 85 mg g^{-1} for Cs^+, Co^{2+} and Eu^{3+}, respectively. The corresponding maximum adsorption capacity of Sb_2O_3/P(AAm-SSS) nanocomposite found to be 90, 75 and 72 mg g^{-1}. From the previous study, the maximum TiO_2/(P (AAm–SSS) nanocomposite capacities for Cs^+, Co^{2+} and Eu^{3+} were found to be 120, 100.9 and 85.7 mg/g, respectively. The latter Sb_2O_3/P(AAm-SSS) nanocomposite values were found to be less than presented by ZnO/P (AAm-SSS) nanocomposite. The variation in the maximum metal adsorption capacity for the three investigated elements indicated that the sorption process is not only dependent on the surface characteristics of the ZnO/P(AAm-SSS) nanocomposite and Sb_2O_3/P(AAm-SSS) nanocomposite (physical sorption) but also correlated to the chemical interaction between the function groups of the nanocomposites and the metal ions. This chemical interaction is stronger with the monovalent Cs ions than that occurred with divalent Co ions and trivalent Eu ions. This interaction is mainly attributed to the presence of sulfonic acid groups (–SO_3Na) and amino groups (–NH_2) as shown previously by FTIR results.

4. Conclusions

Gamma irradiation has been successfully used to prepare ZnO/P(AAm-SSS) and Sb_2O_3/P(AAm-SSS) nanocomposites with enhancement of thermal properties. The addition of metal oxide nanoparticles (ZnO or Sb_2O_3) to synthetic polymers increased the removal capabilities of Cs^+, Co^{2+} and Eu^{3+}. It was found that ZnO nanoparticles embedded in polymeric matrix exhibit higher Cs^+, Co^{2+} and Eu^{3+} ions removal capability than Sb_2O_3/P(AAm-SSS) nanocomposite.

References

[1] R. Rahman, H. Ibrahium, Y.-T. Hung, Liquid radioactive wastes treatment: a review, Water, 3 (2011) 551–565.
[2] Y. Li, S. Wang, Q. Wang, M. Xing, Enhancement of fracture properties of polymer composites reinforced by carbon nanotubes: A molecular dynamics study, Carbon, 129 (2018) 504–509.
[3] M. Yurddaskal, E. Celik, Effect of halogen-free nanoparticles on the mechanical, structural, thermal and flame retardant properties of polymer matrix composite, Comp. Struct., 183 (2018) 381–388.
[4] Y. Zare, Study of nanoparticles aggregation/agglomeration in polymer particulate nanocomposites by mechanical properties, Composites Part A: Appl. Sci. Manufact., 84 (2016) 158–164.
[5] S. Mahdavi, M. Jalali, A. Afkhami, Removal of heavy metals from aqueous solutions using Fe_3O_4, ZnO, and CuO nanoparticles, J. Nanopart. Res., 14 (2012) 846.
[6] X. Wang, W. Cai, S. Liu, G. Wang, Z. Wu, H. Zhao, ZnO hollow microspheres with exposed porous nanosheets surface: structurally enhanced adsorption towards heavy metal ions, Colloids Surfaces A: Physicochem. Eng. Asp., 422 (2013) 199–205.
[7] S. Singh, K. Barick, D. Bahadur, Novel and efficient three dimensional mesoporous ZnO nanoassemblies for envirnomental remediation, Int. J. Nanosci., 10 (2011) 1001–1005.
[8] K.Y. Kumar, H. Muralidhara, Y.A. Nayaka, J. Balasubramanyam, H. Hanumanthappa, Hierarchically assembled mesoporous ZnO nanorods for the removal of lead and cadmium by using differential pulse anodic stripping voltammetric method, Powder Technol., 239 (2013) 208–216.
[9] J.H. Lee, B.S. Kim, J.C. Lee, S. Park, Removal of Cu^{++} ions from aqueous Cu-EDTA solution using ZnO nanopowder, Materials Science Forum, Trans Tech Publ, 2005, pp. 510–513.
[10] M.H. Huang, S. Mao, H. Feick, H. Yan, Y. Wu, H. Kind, E. Weber, R. Russo, P. Yang, Room-temperature ultraviolet nanowire nanolasers, Science, 292 (2001) 1897–1899.
[11] T.B. Massalski, J. Murray, Binary phase diagrams, ASM International, (1990) 1096.
[12] C. Xu, C.H. Woo, S. Shi, Formation of CuO nanowires on Cu foil, Chem. Phys. Lett., 399 (2004) 62–66.

[13] A.S. Khanna, Introduction to high temperature oxidation and corrosion, ASM international, 2002.
[14] M. Nalin, Y. Messaddeq, S. Ribeiro, M. Poulani, V. Briois, Photosensitivity in antimony based glasses, Paris Univ (France), 2001.
[15] N. Sahoo, K. Apparao, Process-parameter optimization of Sb_2O_3 films in the ultraviolet and visible region for interferometric applications, Appl. Phys. A: Mater. Sci. Process., 63 (1996) 195–202.
[16] K. Ozawa, Y. Sakka, M. Amano, Preparation and electrical conductivity of three types of antimonic acid films, J. Mater. Res., 13 (1998) 830–833.
[17] D. Dzimitrowicz, J. Goodenough, P. Wiseman, AC proton conduction in hydrous oxides, Mater. Res. Bull., 17 (1982) 971–979.
[18] P.R. Chang, J. Yu, X. Ma, Fabrication and characterization of Sb_2O_3/carboxymethyl cellulose sodium and the properties of plasticized starch composite films, Macromol. Mater. Eng., 294 (2009) 762–767.
[19] C. Xie, J. Hu, R. Wu, H. Xia, Structure transition comparison between the amorphous nanosize particles and coarse-grained polycrystalline of cobalt, Nanostruct. Mater., 11 (1999) 1061–1066.
[20] Z. Zhang, L. Guo, W. Wang, Synthesis and characterization of antimony oxide nanoparticles, J. Mater. Res., 16 (2001) 803–805.
[21] C. Ye, G. Wang, M. Kong, L. Zhang, Controlled synthesis of Sb_2O_3 nanoparticles, nanowires, and nanoribbons, J. Nanomater., 2006 (2006).
[22] J. Zhang, L. Gao, Synthesis and characterization of antimony-doped tin oxide (ATO) nanoparticles by a new hydrothermal method, Mater. Chem. Phys., 87 (2004) 10–13.
[23] X.Y. Chen, H.S. Huh, S.W. Lee, Hydrothermal synthesis of antimony oxychloride and oxide nanocrystals: $Sb_4O_5Cl_2$, $Sb_8O_{11}C_{12}$, and Sb_2O_3, J. Solid State Chem., 181 (2008) 2127–2132.
[24] Y. Liu, Y. Zhang, M. Zhang, W. Zhang, Y. Qian, L. Yang, C. Wang, Z. Chen, Preparation of nanocrystalline antimony oxide powders by use of γ-ray radiation—oxidization route, Mater. Sci. Eng.: B, 49 (1997) 42–45.
[25] A.K. Jha, K. Prasad, K. Prasad, A green low-cost biosynthesis of Sb_2O_3 nanoparticles, Biochem. Eng. J., 43 (2009) 303–306.
[26] R. Khalili, F. Shabanpour, H. Eisazadeh, Synthesis of polythiophene/Sb_2O_3 nanocomposite using sodium dodecylbenzenesulfonate for the removal of Pb(II), Adv. Polym. Technol., 33 (2014).
[27] J. Ramkumar, S. Chandramouleeswaran, B. Naidu, V. Sudarsan, Antimony phosphate nanoribbons: sorbents for uptake of uranyl ion, J. Radioanal. Nucl. Chem., 298 (2013) 1845–1855.
[28] N. Pandey, S. Shukla, N. Singh, Water purification by polymer nanocomposites: an overview, Nanocomposites, 3 (2017) 47–66.
[29] J. Yin, B. Deng, Polymer-matrix nanocomposite membranes for water treatment, J. Membr. Sci., 479 (2015) 256–275.
[30] R. Ayoub, Adsorption behavior and kinetics of exchange of Co^{2+} and Eu^{3+} ions on polymer composite ion exchanger, Separ. Sci. Technol., 51 (2016) 229–236.
[31] P. Scherrer, Nachrichten von der Gesellschaft der Wissenschaften zu Göttingen, Mathematisch-Physikalische Klasse, 2 (1918) 98–100.
[32] J.-F. Li, Z.-L. Xu, H. Yang, L.-Y. Yu, M. Liu, Effect of TiO_2 nanoparticles on the surface morphology and performance of microporous PES membrane, Appl. Surf. Sci., 255 (2009) 4725–4732.
[33] B.L. Rivas, B. Urbano, C. Muñoz, Metal ion sorption properties of water-insoluble resins based on sodium styrene sulfonate and different comonomers, Polym. Bull., 68 (2012) 1537–1549.
[34] Z. Deng, F. Tang, D. Chen, X. Meng, L. Cao, B. Zou, A simple solution route to single-crystalline Sb_2O_3 nanowires with rectangular cross sections, J. Phys. Chem. B, 110 (2006) 18225–18230.
[35] M. Nalin, Y. Messaddeq, S. Ribeiro, M. Poulain, V. Briois, G. Brunklaus, C. Rosenhahn, B. Mosel, H. Eckert, Structural organization and thermal properties of the Sb_2O_3–$SbPO_4$ glass system, J. Mater. Chem., 14 (2004) 3398–3405.
[36] Y. Wei, H.-Q. Chu, B.-Z. Dong, X. Li, S.-J. Xia, Z.-M. Qiang, Effect of TiO_2 nanowire addition on PVDF ultrafiltration membrane performance, Desalination, 272 (2011) 90–97.
[37] Y. Agrawal, A. Shashimohan, A. Biswas, Studies on antimony oxides: Part I: Thermal analysis of Sb_2O_3 in air, nitrogen and argon, J. Thermal Anal. Calorim., 7 (1975) 635–641.
[38] M.S. Lashkenari, B. Davodi, H. Eisazadeh, Removal of arsenic from aqueous solution using polyaniline/rice husk nanocomposite, Korean J. Chem. Eng., 28 (2011) 1532–1538.